# Dependence of Snow Gauge Collection Efficiency on Snowflake Characteristics

JULIE M. THÉRIAULT,* ROY RASMUSSEN, KYOKO IKEDA, AND SCOTT LANDOLT

*National Center for Atmospheric Research,[+] Boulder, Colorado*

(Manuscript received 25 May 2011, in final form 26 October 2011)

ABSTRACT

Accurate snowfall measurements are critical for a wide variety of research fields, including snowpack monitoring, climate variability, and hydrological applications. It has been recognized that systematic errors in snowfall measurements are often observed as a result of the gauge geometry and the weather conditions. The goal of this study is to understand better the scatter in the snowfall precipitation rate measured by a gauge. To address this issue, field observations and numerical simulations were carried out. First, a theoretical study using finite-element modeling was used to simulate the flow around the gauge. The snowflake trajectories were investigated using a Lagrangian model, and the derived flow field was used to compute a theoretical collection efficiency for different types of snowflakes. Second, field observations were undertaken to determine how different types, shapes, and sizes of snowflakes are collected inside a Geonor, Inc., precipitation gauge. The results show that the collection efficiency is influenced by the type of snowflakes as well as by their size distribution. Different types of snowflakes, which fall at different terminal velocities, interact differently with the airflow around the gauge. Fast-falling snowflakes are more efficiently collected by the gauge than slow-falling ones. The correction factor used to correct the data for the wind speed is improved by adding a parameter for each type of snowflake. The results show that accurate measure of snow depends on the wind speed as well as the type of snowflake observed during a snowstorm.

## 1. Introduction

Large uncertainties are often observed in precipitation measurements, especially for solid precipitation (e.g., Groisman et al. 1991; Groisman and Legates 1994; Yang et al. 1995; Goodison et al. 1998). An accurate measure of snowfall amount is critical because it is directly linked to a better understanding of the global water cycle. Discrepancies in snowfall measurement may lead to uncertainties in the analysis of climate variability and the verification of climate models (Yang et al. 2005). Over a shorter time scale, the precise amount of snow falling on the ground has an impact on surface and air transportation. To be more specific, the determination of real-time precipitation type and intensity affects the decision making for aircraft ground deicing operations (Rasmussen et al. 2001).

Solid precipitation measurement is challenging because technical factors, such as gauge geometry and capping of snow, may bias the measured precipitation quantity. Yang et al. (2005) stated that correction factors needed to be applied to the data to account for wetting evaporation losses and wind-induced error. The wind-induced error is caused by the deformation of the airflow due to the gauge geometry. Sevruk et al. (2009) showed that the higher the wind speed is the lower is the precipitation rate recorded by the gauge because of snowflakes blowing over or around the gauge, making wind the most important contributor to the uncertainties.

A shield is typically installed around the precipitation gauge to reduce the effects of the wind on the gauge collection efficiency (Yang et al. 1999). Many different gauge and shield configurations have been studied in the past, and their measurements have been characterized under different wind speeds (e.g., Nipher 1878; Alter 1937; Yang et al. 1998; Hanson et al. 2004; Smith 2009; Rasmussen

* Current affiliation: Département des sciences de la Terre et de l'atmosphère, Université du Québec à Montréal, Montréal, Québec, Canada.

[+] The National Center for Atmospheric Research is sponsored by the National Science Foundation.

*Corresponding author address:* Julie M. Thériault, Université du Québec à Montréal, Département des sciences de la Terre et de l'atmosphère, Case postale 8888, Succursale Centre-ville, Montréal, QC H3C 3P8, Canada.
E-mail: theriault.julie@uqam.ca

DOI: 10.1175/JAMC-D-11-0116.1

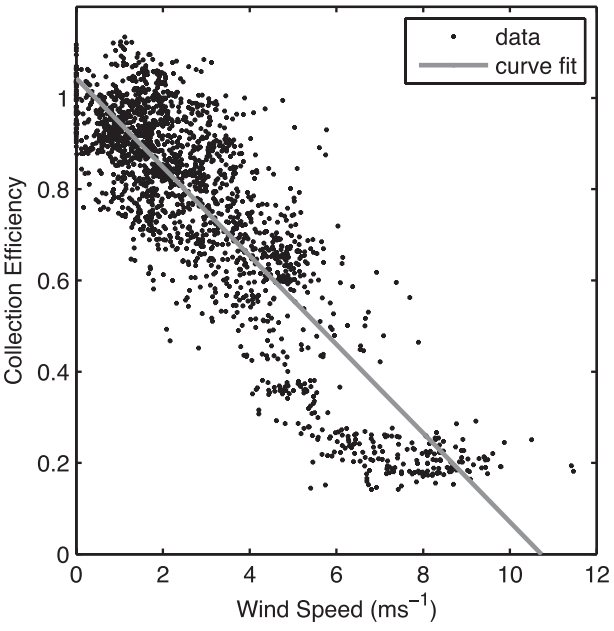


FIG. 1. The collection efficiency of a Geonor in a single Alter shield with respect to a Geonor in a DFIR as a function of wind speed from December 2009 to March 2010. The data (dots) are averaged over 10 min. A linear curve fit of the data is indicated by the gray line. There are a total of 1870 data points during approximately 20 weather events.

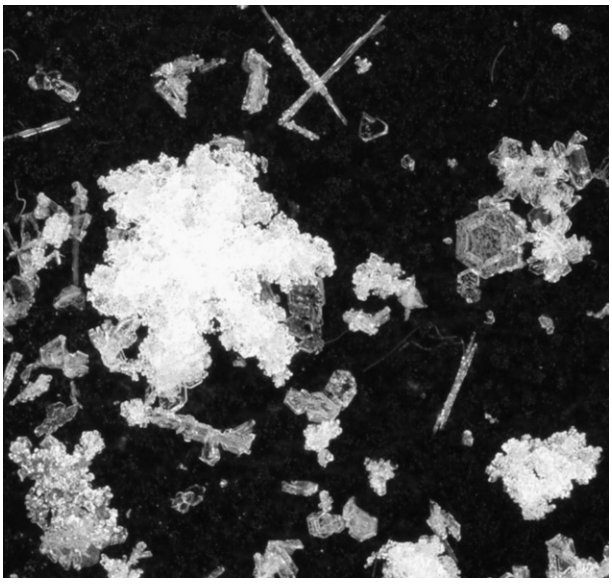

FIG. 2. Example of the different crystal types that can be observed simultaneously at the surface.

et al. 2012). In 1985, the World Meteorological Organization Commission on Instruments and Methods of Observation designated the Double Fence Intercomparison Reference (DFIR) as the standard shield for precipitation measurements (Goodison et al. 1998). Therefore, the best precipitation-rate estimate is assumed to be measured by the gauge in a DFIR.

To study the performance of a gauge or gauge–shield configuration, the collection efficiency needs to be computed. The collection efficiency is defined as the ratio of the precipitation rate measured by the gauge to the best estimate of the precipitation rate. Figure 1 shows the collection efficiency of a Geonor, Inc., gauge (hereinafter "Geonor") placed in a single Alter shield with respect to a Geonor in a DFIR. It illustrates the large scatter in the data as a function of wind speed. Note that for a single wind speed value the error can be as high as 50%. A correction factor is currently used to account for the decrease in collection efficiency with increasing wind speed. This correction factor, which is derived from the data used in Rasmussen et al. (2001), depends on the gauge–shield configuration. The corrected data also show scatter, however, especially during high-wind events.

Because the gauge is an obstacle to the natural airflow pattern, an updraft and horizontal accelerations may be produced at the top of the gauge that cause the snowflakes to blow over the top of the gauge. The strength of the updraft depends on the horizontal wind speed and may cause the particle to deviate from its original trajectory (Rasmussen et al. 2012). The shield around the gauge acts to slow the wind speed and, in turn, decreases the strength of the updraft created at the gauge orifice and may induce turbulence. Nespor and Sevruk (1999) have addressed this issue by simulating raindrop trajectories in the vicinity of the gauge. Goodison et al. (1998) made initial studies on snowflake trajectories. They showed that the lighter the snowflakes are the higher is the wind-induced error for two different precipitation gauges [automatic station tipping-bucket (ASTA) and Hellman].

Measuring snowfall amount is also complicated because it is common to observe many different types of snowflakes simultaneously at the surface (Fig. 2). Many studies have examined the characteristics of the various types of snowflakes often observed during winter storms (e.g., Sekhon and Srivastava 1970; Locatelli and Hobbs 1974; Passarelli 1978; Brandes et al. 2007). Yuter et al. (2006) showed that the snowflake terminal velocity is highly variable and may vary from 0.5 to 3 m s$^{-1}$. This variability may affect the gauge collection efficiency.

Given the importance of accurately measuring snowfall amount, the effect of snowflake characteristics on gauge collection was investigated. The goal of the study is to understand better the scatter in the collection efficiency of a Geonor in a single Alter shield for a given wind speed. We chose the Alter shield because it is one of the five most commonly used shields.

To address this issue, snowflakes falling inside and outside of a Geonor snow gauge were collected and

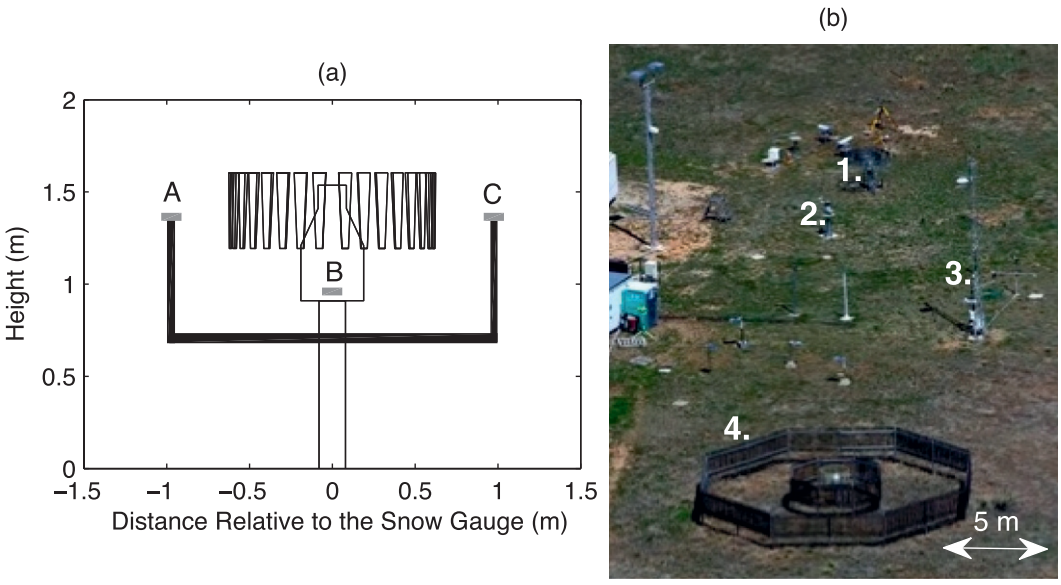


FIG. 3. (a) A schematic of the Geonor placed on a stand. Snow collection pads (gray) are placed on each side of the snow gauge (A and C) and in the gauge (B). (b) The Marshall test bed (Rasmussen et al. 2012). The location of the experimental setup (label 2) described in (a) with respect to the weather instruments used in this study: label 1 is the Geonor in a single Alter shield, label 3 is the 2-m anemometer tower, and label 4 is the Geonor in a DFIR.

photographed during snowfall events. Each snowflake was analyzed systematically to determine its characteristics such as shape and type. Also, a well-equipped test site allowed the unique snowflake datasets used in this study to be compared with observed weather conditions. In addition to the field experiments, numerical simulations were performed on the relationship of the collection efficiency and terminal velocity.

The paper is organized as follows. Sections 2 and 3 describe the experimental design, including the data collected in the field and the numerical simulations conducted, respectively. Section 4 investigates the theoretical collection efficiency for the different crystal patterns. Observations recorded in the field are summarized and discussed in section 5. The theoretical results are compared with observations in section 6. The conclusions are in section 7.

## 2. Observational data

During the winter of 2009/10, detailed snowflake observations were conducted at the Marshall Field Site, near Boulder, Colorado. The site is maintained by the National Center for Atmospheric Research and is a test bed for a number of weather instruments and precipitation gauges (Rasmussen et al. 2012). The purpose of the experiment was to collect snowflakes inside and outside a Geonor gauge and analyze their characteristics to explain the scatter in the snowfall measurement of the gauge. The Geonor gauge is based on vibrating-wire technology (Bakkehoi et al. 1985).

Figure 3a shows a schematic of the experimental setup. The experiment consisted of collecting snowflakes on a collection pad, covered by black velvet, that has dimensions of 20 cm $\times$ 11 cm. Two collection pads were placed on tray A and C, outside the gauge as shown in Fig. 3a. One collection pad was placed inside the gauge itself (tray B). The collection pads were exposed to the environmental conditions for a short time period (10–20 s) to prevent snowflakes from overlapping on the collection pads. The collected snowflakes were then photographed inside an unheated trailer. The experiment was repeated every 20 min during snowfall events. To address the impact of the shield on the collection efficiency, a single Alter shield was added between the trays (Fig. 3a, A and C) and the gauge for every other storm.

Once the snowflakes collected, they were photographed in a systematic manner using a Pentax digital single-lens reflex camera with a 100-mm macro lens. The camera was mounted on a tripod and was always placed at the same distance from the collection pad to give the same pixel size for every picture. Three pictures were taken at the center of the long side of each collection pad. Once the picture was taken, the different types of snowflakes observed on each collection pad were recorded.

Nearly 2400 pictures were analyzed meticulously by hand to determine if snowflakes were overlapping. For consistency, for every image ignored the ones taken at the same time on the two other collection pads were also ignored. Furthermore, the main snowflake type on each image was recorded and was compared with the manual observations of snowflake types. This step has been repeated by two scientists to confirm the main type of snowflake at a given time. They were separated into four primary types: dendrite, radiating assemblage of plates, graupel, and irregular ice particles. These types of snowflakes were classified into two main categories of snow: dry and wet/rimed snowflakes. The difference between these types of snowflakes is mainly the terminal velocity and density. Dendrites and radiating assemblage of plates are considered to be ''dry'' snow, which has a terminal velocity of $\sim$1 m $s^{-1}$. Graupel and irregular ice particles are considered to be ''wet/rimed'' snow, which is relatively more dense and falls faster ($\sim$2 m $s^{-1}$).

After the quality control of the pictures, the images were processed using Matlab proprietary software. A program was written to detect and measure each snowflake and to compute snowflake characteristics such as major and minor axis, equivalent diameter, and eccentricity. The diameter used in the analysis is the equivalent diameter, which is defined as the diameter of a circle of the same surface area of the detected snowflake. The snowflake characteristics were then compared with the wind speed approximately at gauge height (2-m anemometer tower) and the precipitation rate measured by the Geonor in the single Alter and the Geonor in the DFIR, all averaged over 10 min. Because the snowflakes were photographed at every 20 min, we have three samples per hour. The location of the weather instruments used for this study relative to the experimental setup (Fig. 3a) is depicted in Fig. 3b. All the instruments used are within a 20-m radius of each other. Only the samples associated with a precipitation rate (Geonor in the DFIR) of $>$0.3 mm $h^{-1}$ were considered.

Data were collected during many storms in the winter 2009/10, but on the basis of the quality-control review, only five storms are presented in this study. The shield was used during four of the five storms analyzed. Table 1 summarizes for each event the dates, number of samples, precipitation rates, wind speeds, and whether the gauge was shielded.

By using these observations and associated gauge measurements, the collection efficiency of precipitation gauges and weather conditions were compared with the snowflake characteristics and types. The 20 February 2010 event is used to describe the effects of the crystal type on the snow gauge collection efficiency. Data from all of the storms were then combined to compare with the theoretical results.

TABLE 1. Summary of each storm for which crystal-type characteristics were collected during winter 2009/10. The abbreviation No. is the number of time samples, $R$ is the range of the precipitation rate (mm $h^{-1}$) calculated from the Geonor in the DFIR, and $V$ is the range of the average wind speed (m $s^{-1}$) measured during each event. Note that $R$ and $V$ are averaged over 10 min.

| Time (UTC) | No. | $R$ | $V$ | Shielded |
|---|---|---|---|---|
| 0000 22 Dec–1200 23 Dec 2009 | 21 | 0.32–1.3 | 0.9–4.7 | No |
| 1640 7 Feb–0420 8 Feb 2010 | 12 | 0.32–1.05 | 0–1.8 | Yes |
| 1100–1520 14 Feb 2010 | 9 | 0.32–1.3 | 1.9–3.2 | Yes |
| 0040–0600 19 Feb 2010 | 14 | 0.31–1.57 | 1.5–4.4 | Yes |
| 2300 20 Feb–0840 21 Feb 2010 | 16 | 0.35–0.92 | 2.5–4.4 | Yes |

## 3. Theoretical study

To simulate a theoretical gauge collection efficiency, an approach with the following three steps was taken:

1) determine the flow around a shielded gauge using computational fluid dynamics software,
2) compute particle trajectories with a Lagrangian model, and
3) calculate a theoretical collection efficiency on the basis of the number of snowflakes falling inside the gauge.

These steps are discussed in detail below.

### *a. Fluid dynamics modeling*

The flow around the shielded gauge was simulated using the ''Fluent'' computational fluid dynamics software package from Ansys, Inc. (http://www.ansys.com/Products/Simulation+Technology/Fluid+Dynamics/ANSYS+Fluent). To simulate the flow in Fluent, the geometry and meshing of the Geonor in a single Alter shield was constructed using ''Gambit,'' an Ansys subprogram designed to work with Fluent. This software has been used in many studies linked to a wide variety of fields. Newman and Kucera (2005) used it to study the airflow around a disdrometer and to demonstrate that the airflow produced by Fluent agreed well with observations. The Fluent software solves the equations of conservation of mass and momentum. Additional equations are considered to account for heat transfer or compressibility depending on the problem addressed. In a similar way, transport equations are solved for turbulent flow. Fluent provides three models to solve for a $k$–epsilon turbulent flow. In this study we chose to use the standard $k$-epsilon model, which solves for the turbulence kinetic energy $k$ and its dissipation rate epsilon. More details are found in the user's manual (https://www.sharcnet.ca/Software/Fluent12/pdf/th/flth.pdf).

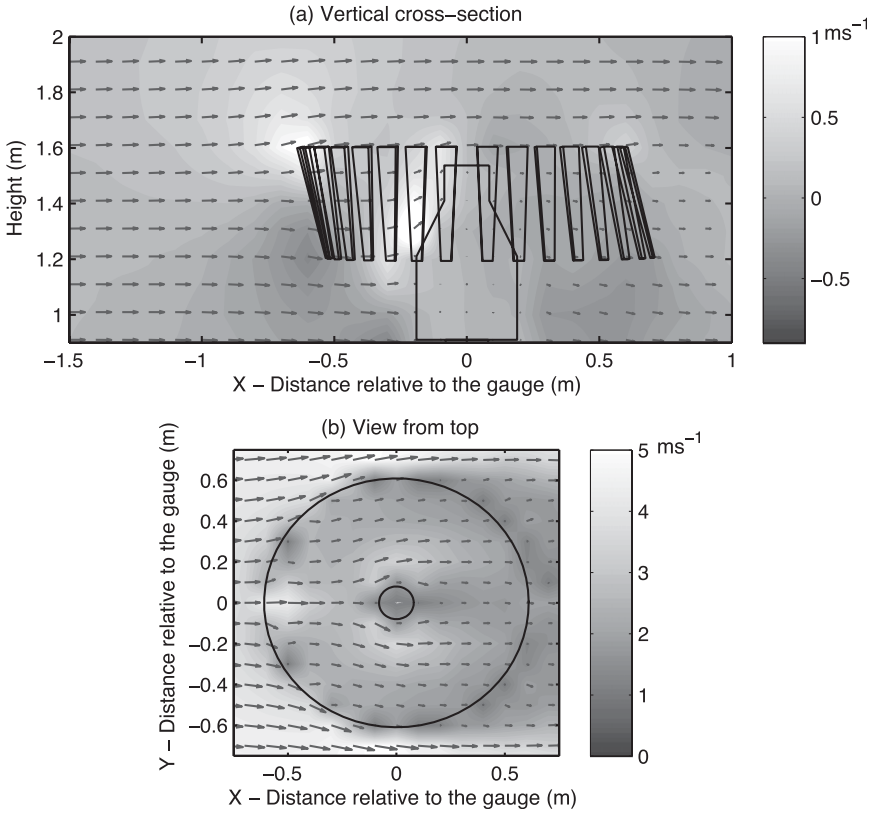


FIG. 4. (a) An example of a cross section of the flow parallel to the wind speed (gray arrows). The initial wind speed is 5 m $s^{-1}$, with a slat orientation of 15° with respect to vertical in the same direction of the wind. The horizontal wind speed parallel to the cross section (m $s^{-1}$) is indicated by the arrows, and the vertical air velocity values are indicated by the gray shading. The geometry of the gauge and orientation of the slats are indicated by the black lines. (b) The flow viewed from 2 cm above the gauge. The wind speed parallel to the cross section is indicated by the lengths of the gray arrows and by the gray shading (m $s^{-1}$), and the wind direction is indicated by the orientation of the arrows. The shield around the gauge is the larger circle, and the orifice of the gauge is the small circle.

A few assumptions on the shield geometry were made to facilitate the simulation of the flow. The single Alter shield is composed of 32 slats hanging in a circle around the gauge that move with the wind. For these simulations, it is assumed that the slats are motionless but are hung at different angles with respect to vertical in the direction of the wind as a function of the wind speed. Figure 4 illustrates a vertical cross section of the gauge–shield geometry. The flow simulations have been performed in three dimensions. A square perimeter was defined around the gauge–shield geometry (20 m × 20 m × 20 m) composed of approximately 350 000 cells, with refinement near the gauge–shield configuration. All of the boundaries of the perimeter were defined as solid walls except for the inflow and the outflow sides of the box. These boundary conditions allowed an environment around the gauge to be of sufficient size such that the wind flow was laminar before encountering the gauge–shield combination.

Once the gauge–shield geometry was defined and meshed, Fluent was used to simulate the flow in the vicinity of the snow gauge. Several conditions were defined within the simulation. First, the fluid in the box was defined as air (1 kg $m^{-3}$). Second, a wind speed value was initialized on the inflow wall. Constant wind speed values of 1–10 m $s^{-1}$ were tested with increments of 1 m $s^{-1}$. Third, the flow model type was set to *k*–epsilon turbulent. For comparison, the experiment was repeated with a laminar flow to study the effect of turbulent flow on the collection efficiency of the gauge. Last, Fluent was run until it converged to a steady-state flow.

To address the deflection the slats would have in actual wind flow, the angle of the slats was adjusted to varying degrees depending on the wind speed. For wind speeds between 1 and 5 m $s^{-1}$, the slats were assumed to be oriented 15° with respect to vertical (Fig. 4a). The slats were assumed to be 30° with respect to vertical for

TABLE 2. Definition of the parameters to compute the terminal velocity, density, volume, and area of each snowflake type. The general form of the equation is $Y_X(D) = a_X D^{b_X}$. The values are taken from Rasmussen et al. (1999). The subscript $T$ is for terminal velocity, $V$ is for volume, $\rho$ is for density, and $A$ is for cross-sectional area.

| Crystal types | Symbol | $a_T$ | $b_T$ | $a_V$ | $b_V$ | $a_\rho$ | $b_\rho$ | $a_A$ | $b_A$ |
|---|---|---|---|---|---|---|---|---|---|
| Radiating assemblage of plates | RP | 60 | 0.37 | 0.0028 | 1.8 | 0.49 | 0 | $\pi/4$ | 2 |
| Dendrite | DE | 55 | 0.48 | 0.0012 | 2.29 | 0.5 | 0 | $\pi/4$ | 2 |
| Heavily rimed dendrite | HD | 162 | 0.53 | 0.0023 | 1.7 | 0.58 | 0 | $\pi/4$ | 2 |
| Hexagonal plates | HP | 297 | 0.86 | 0.0417 | 3.31 | 0.9 | 0 | $\pi/4$ | 2 |
| Lump graupel | LG | 733 | 0.89 | $\pi/6$ | 3 | 0.9 | 0 | $\pi/4$ | 2 |
| Dry snow | DS | 107 | 0.2 | $\pi/6$ | 3 | 0.017 | −1 | $\pi/4$ | 2 |
| Wet snow | WS | 214 | 0.2 | $\pi/6$ | 3 | 0.072 | −1 | $\pi/4$ | 2 |

wind speeds between 6 and 10 m s$^{-1}$. For a given wind speed, the flow seems to be slightly sensitive to the orientation of the slats. For example, at 5 m s$^{-1}$ the flow pattern is similar with the same order observed for the vertical air velocity (updraft). There are some differences in the size of the area where the maximum wind speed in observed, however. Further studies should be conducted to explore in detail this issue.

### b. Lagrangian model

A Lagrangian model was developed to study the snowflake trajectory. Nespor and Sevruk (1999) developed a similar Lagrangian model to study raindrop trajectory around a precipitation gauge. The flow field obtained with Fluent was used to initialize the model.

The equation of motion is

$$V_s\rho_s\mathbf{a}_s = -C_dA_s\rho_a 0.5(\mathbf{v}_s - \mathbf{v}_a)|\mathbf{v}_s - \mathbf{v}_a| + V_s(\rho_s - \rho_a)\mathbf{g}, \tag{1}$$

where $\mathbf{a}_s$ is the snowflake acceleration, $V_s$ is the volume of the snowflake, $\rho_s$ is the snow density, $\rho_a$ is the air density, $C_d$ is the drag coefficient [see Eq. (8) below], $A_s$ is the cross-sectional area normal to the flow, $\mathbf{v}_s$ is the velocity of the snowflake, $\mathbf{v}_a$ is the velocity of the fluid, $\mathbf{g}$ is the gravity acceleration, and $|\mathbf{v}_s - \mathbf{v}_a|$ is the magnitude of the velocity vector:

$$|\mathbf{v}_s - \mathbf{v}_a| = [(u_s - u_a)^2 + (v_s - v_a)^2 + (w_s - w_a)^2]^{1/2}, \tag{2}$$

where $u_x$ is the velocity along the $x$ axis, $v_x$ is the velocity along the $y$ axis, and $w_x$ is the velocity along the $z$ axis for the snowflake (subscript $x = s$) and the environmental air (subscript $x = a$). Because the gravity force is only acting along the $z$ axis, the components of the acceleration vector are

$$a_x = -\frac{1}{2}C_dA_s\frac{\rho_a}{V_s\rho_s}(\mathbf{u}_s - \mathbf{u}_a)|\mathbf{v}_s - \mathbf{v}_a|, \tag{3}$$

$$a_y = -\frac{1}{2}C_dA_s\frac{\rho_a}{V_s\rho_s}(\mathbf{v}_s - \mathbf{v}_a)|\mathbf{v}_s - \mathbf{v}_a|, \quad \text{and} \tag{4}$$

$$a_z = -\frac{1}{2}C_dA_s\frac{\rho_a}{V_s\rho_s}(\mathbf{w}_s - \mathbf{w}_a)|\mathbf{v}_s - \mathbf{v}_a| + \frac{(\rho_s - \rho_a)}{\rho_s}g. \tag{5}$$

The initial particle velocity is assumed to be the terminal velocity ($z$ axis) and the horizontal wind speed ($x$ axis). The particle velocity along the $y$ axis is zero. Given the initial position and velocity of the particle, the acceleration of the particle is computed and, in turn, the three-dimensional location of the snowflake at each time step is determined. On the basis of sensitivity tests, the time step was set to 0.001 s. Note also that the effect of turbulence on the particle is only considered by the turbulent flow obtained by Fluent. This assumption differs from Nespor and Sevruk (1999), who added a turbulent effect to the drag coefficient.

### c. Snowflake characteristics

The equations of motion given in Eqs. (3)–(5) illustrate the impact of snowflake type on its acceleration. The drag coefficient $C_d$ also depends on the snowflake type and size (Pruppacher and Klett 1997) and is defined as

$$C_D = \frac{2V_s(\rho_s - \rho_a)g}{A_s\rho_a v_T^2}, \tag{6}$$

where $V_s$ is the volume, $A_s$ is the area, $g$ is the gravity constant, $\rho_s$ is the snow density, $\rho_a$ is the air density, and $v_T$ is the terminal velocity of the snowflake.

From Rasmussen et al. (1999), the general form of the volume, cross sectional, density, and terminal velocity parameters are

$$Y_X(D) = a_X D^{b_X}, \tag{7}$$

where $D$ is the snowflake diameter, and $a_X$ and $b_X$ are the parameters that are summarized in Table 2. The

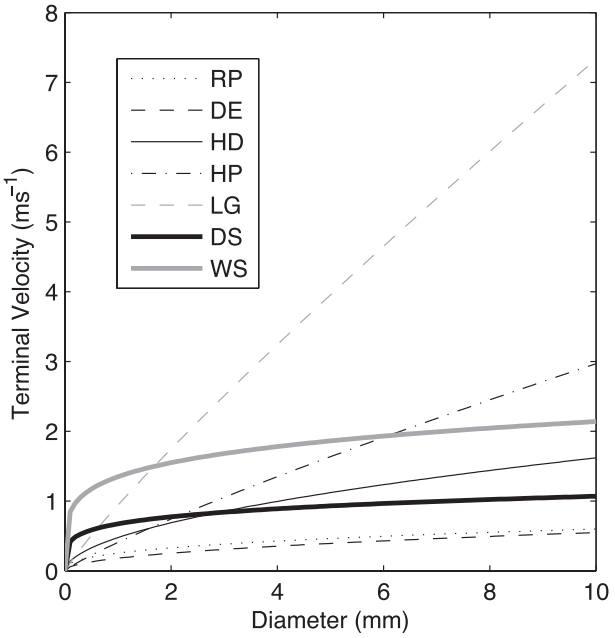


FIG. 5. The terminal velocity for each crystal type as a function of diameter. The symbols are summarized in Table 2.

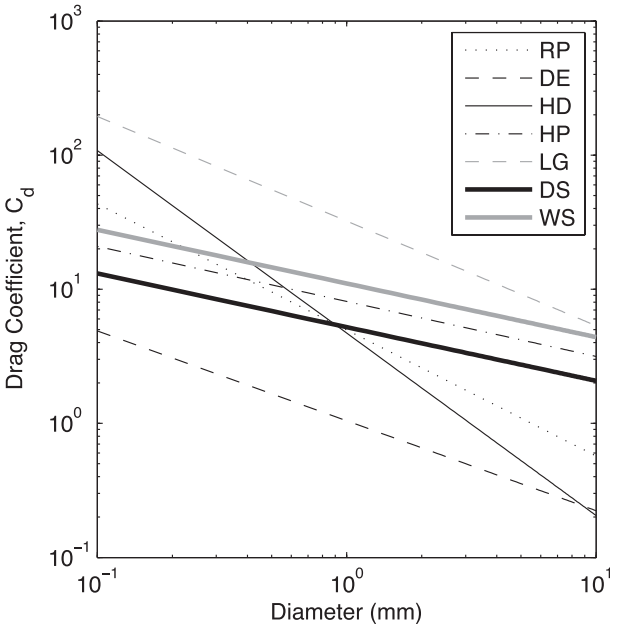


FIG. 6. The drag coefficient for the different crystal types as a function of diameter. The symbols are summarized in Table 2.

volume and density of each snowflake also vary as a function of the snowflake diameter. In a similar way, the cross-sectional area is assumed to be a circle for all of the snowflake types studied. Given that the snowflake shape is highly variable, this is a reasonable assumption.

By merging Eq. (7) into Eq. (6), the drag coefficient can be written as

$$C_D = \frac{2ga_V a_\rho}{a_A \rho_{\text{air}} a_T} D^{b_V + b_\rho - b_A - 2b_T}, \tag{8}$$

where the subscript $V$ refers to the volume of the snowflake, $T$ is for the terminal velocity, $A$ is the cross-sectional area, and $\rho$ is for the density. The values are also given in Table 2.

The terminal velocities for the seven snowflake types studied are shown in Fig. 5. The terminal velocity of a dendrite is less than any other snowflake type shown and asymptotically approaches to near a constant value with size. Graupel falls at a relatively higher terminal velocity and generally has higher particle density than other snowflake types.

Figure 6 shows the decrease in the drag coefficient with increasing snowflake diameter. This is because the effect of air resistance is less important and the particle will be less influenced by the horizontal flow. These calculations were done by considering single snowflakes rather than aggregates. According to Eqs. (3), (4), and (5), particles with a high drag coefficient will accelerate more than particles with a smaller drag coefficient. This is consistent with dendrites falling at slower terminal velocities than lump graupel. Also, a slow-falling snowflake has a smaller drag coefficient than a fast-falling snowflake. Note that the shape and density of the snowflake also impact the drag coefficient, where the drag coefficient is typically large for particles with large cross-sectional area and high density.

### *d. Calculation of the collection efficiency*

The collection efficiency is the ratio of the snowfall amount measured by the gauge to the true snowfall measured in a DFIR. To compare the theory with observations, it is assumed that the distortion of the wind in the vicinity of the gauge is negligible.

The ''area method'' is used to compute the collection efficiency of the instrument. It is the ratio of the horizontal area at a given height above the top of the gauge associated with the total number of snowflakes falling into the gauge $A_{\text{inside}}(D)$ to the area of the orifice of the gauge $A_{\text{gauge}}$ (Fig. 3). The area associated with the number of snowflakes falling in the gauge depends on the snowflake characteristics and is never greater than the area of the gauge orifice. For a given snowflake type and wind speed, however, the area concentration of snowflakes will vary. As an analogy between observations and theory, the precipitation rate measured by the Geonor in the single Alter shield refers to $A_{\text{inside}}$ and the measurement by the Geonor in the DFIR is $A_{\text{gauge}}$.

Given an inverse exponential snowflake size distribution (Marshall and Palmer 1948)

$$N(D) = N_0 \exp(-\lambda D), \tag{9}$$

where $N_0$ is the intercept of the size distribution, $D$ is the snowflake diameter, and $\lambda$ is the slope of the size distribution, the theoretical collection efficiency is defined as

$$\mathrm{CE} = \frac{\int_0^{D_{\max}} A_{\mathrm{inside}}(D) N(D)}{\int_0^{D_{\max}} A_{\mathrm{gauge}} N(D)}. \tag{10}$$

To compute the collection efficiency for the different snowflake types, 12 different snowflake diameters were studied for each snowflake type: 0.5, 0.75, 1, 2, 3, 4, 5, 6, 7, 8, 9, and 10 mm. To study the effects of the snowflake size distribution, the intercept of the size distribution remains constant ($N_0 = 5 \times 10^6$ m$^{-4}$) while the slope was varied. This assumption allowed for a more important change in the number concentration of larger snowflake sizes. The intercept was varied over 0.25, 0.5, 1, and 2 mm$^{-1}$. The values were based on Houze et al. (1979), who observed the snow size distribution in different atmospheric conditions.

## 4. Theoretical collection efficiency

### a. Trajectory of snowflakes

Figure 4a shows the flow in the vicinity of the snow gauge. At a height of 2 m, the flow is mostly constant and parallel to the surface. The flow is also constant with a height up to 1 m upstream of the gauge. Because the shielded gauge acts to block the flow, wind speed is higher upstream than downstream of the gauge–shield configuration.

Two major flow deflections are observed in the vicinity of the shielded gauge (Fig. 4a). First, an updraft is observed just upstream of the shield. The slats force the wind to split and create an updraft near their top and a downdraft near their base. Therefore, the trajectory of the snowflake is perturbed upward or downward depending on its location upstream of the shield. Second, the flow between the shield and the gauge is also forced to deviate around the gauge. It creates a secondary updraft near the top of the gauge, which also influences the snowflake trajectory. The updraft created by the shield is stronger than the one created by the gauge because the flow slows down between the shield and the gauge. The view from the top of the gauge (Fig. 4b) also shows the deflection of the flow around the shield. The wind speed decreases inside the shield and also deflects around the orifice of the gauge.

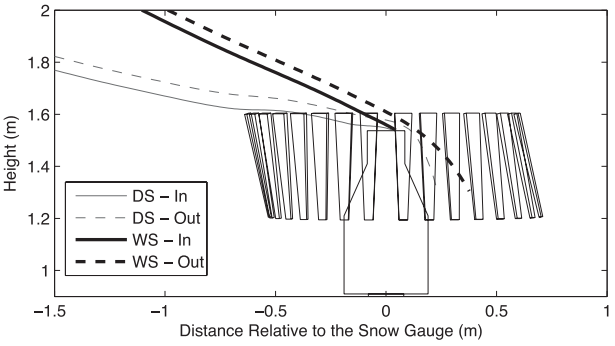


FIG. 7. Trajectories of a 1-mm-diameter dry (DS; gray lines) or wet (WS; black lines) snowflake falling in a flow field of 3 m s$^{-1}$. The solid lines are the trajectories of snowflakes falling into the gauge, and the dashed lines are trajectories that are deflected outside the gauge.

As described in the Lagrangian model, the snowflake trajectory depends on the snowflake characteristics. The main differences between wet/rimed and dry snow are the density and the terminal velocity (Table 2). Figure 7 shows the trajectories of wet/rimed and dry snowflakes of the same size falling inside and outside the gauge. Because dry snow falls more slowly and is less dense than wet/rimed snow, its trajectory follows the streamlines more closely than does that of the wet/rimed snow. The dry snowflake is pushed upward by updrafts located in front of both the shield and the gauge. The snowflake falling inside the gauge arrives at lower heights (gray solid line) in front of the shield when compared with the one falling outside the gauge (gray dashed line). The snowflake falling inside the gauge has just enough momentum to fall into it as compared with the one that has blown over the gauge orifice. The wet/rimed snowflake is not as affected by the flow because it falls faster and the amount of deflection is minimal. The trajectory of the wet snowflake falling outside the gauge is deflected by the flow just above the gauge orifice. Without the effect of the flow on the snowflake, it would have likely fallen inside the gauge.

### b. Collection efficiency and snowflake diameter

According to the snowflake trajectories shown in Fig. 7, the snowflake terminal velocity is an important factor influencing the gauge collection efficiency. In addition, the snowflake size impacts the gauge collection efficiency because larger snowflakes fall faster. The impacts of snowflake size and type are shown in Fig. 8. In general, the collection efficiency of the gauge decreases with increasing wind speed. Large (10-mm diameter) wet/rimed snowflakes lead to a constant collection efficiency

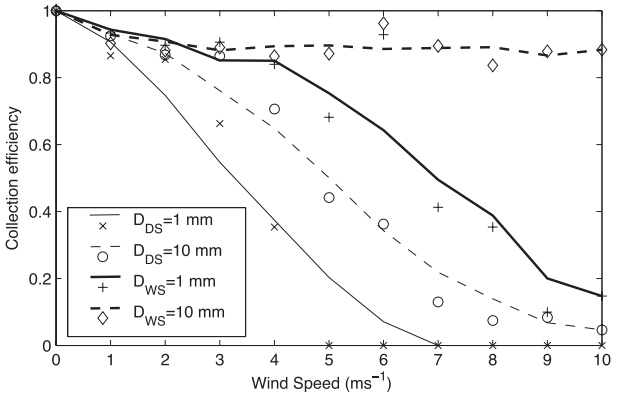


FIG. 8. The collection efficiency of dry ($D_{DS}$; gray lines) and wet/rimed snowflake ($D_{WS}$; black lines) of 1- and 10-mm diameter. The computed collection efficiency is indicated by the markers. The solid (dashed) lines are the smoothed results for 1-mm (10 mm) diameter to show the tendency.

up to at least 10 m s$^{-1}$, however. The collection efficiency of small snowflakes is lower than larger snowflakes of the same type. For example, a 1-mm-diameter dry snowflake has a collection efficiency of 0.4 whereas 0.7 is associated with a 10-mm diameter for the same wind speed (4 m s$^{-1}$). In a similar way, the gauge collection efficiency is also affected by the type of snow. For example, for a 1-mm dry snowflake the collection efficiency is less by almost a factor of 2 than for a 1-mm wet/rimed snowflake falling in a 4 m s$^{-1}$ flow field. For the 10-mm-diameter snowflake, the collection efficiency difference between dry and wet/rimed increases with increasing wind speed.

Whether the snowflake falls into the gauge depends on its trajectory in the vicinity of the gauge. If the snowflake approaches near the shield where the updraft is observed, it will likely deviate from its original trajectory and fall to the ground downstream of the gauge. It has to approach at a precise location above the shielded gauge to have sufficient momentum to fall inside the gauge. This effect helps to explain some of the variability in the computed collection efficiency.

### c. Size distribution of snowflake falling in the gauge

According to the simulations, the snowflake size distribution falling in the gauge can be computed. It was determined using the inverse exponential relation [Eq. (9)], and it is weighted with the area associated with the number of snowflakes falling inside the gauge [$A_{\text{gauge}}(D)$].

Figure 9 shows the size distribution of dry and wet/rimed snowflakes falling inside the gauge for different wind speeds. For dry snow at 0 m s$^{-1}$, the size distribution of snowflakes falling inside and outside the gauge is the same. As the wind speed increases, the minimum size of snowflakes falling inside the gauge increases. There is a difference of 5 mm between the smallest snowflakes falling into the gauge at 4 m s$^{-1}$ when compared with 8 m s$^{-1}$. At 10 m s$^{-1}$, no snowflakes smaller than 10 mm in diameter fall into the gauge. Conversely,

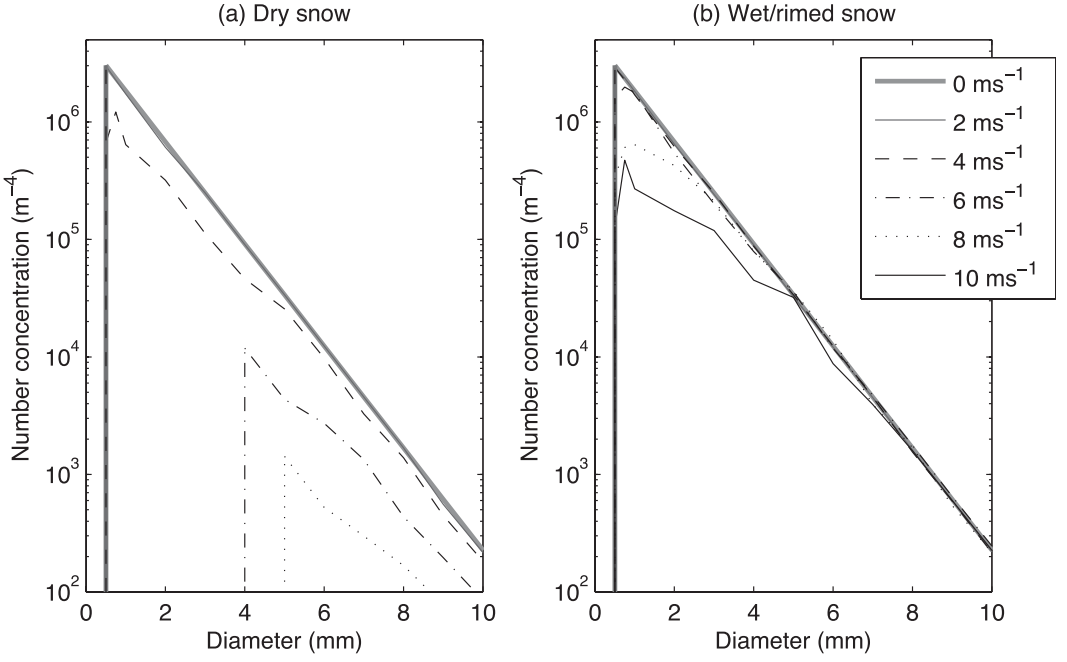


FIG. 9. The size distribution of snowflakes falling inside the gauge when falling through different wind speeds for (a) dry snow and (b) wet snow.

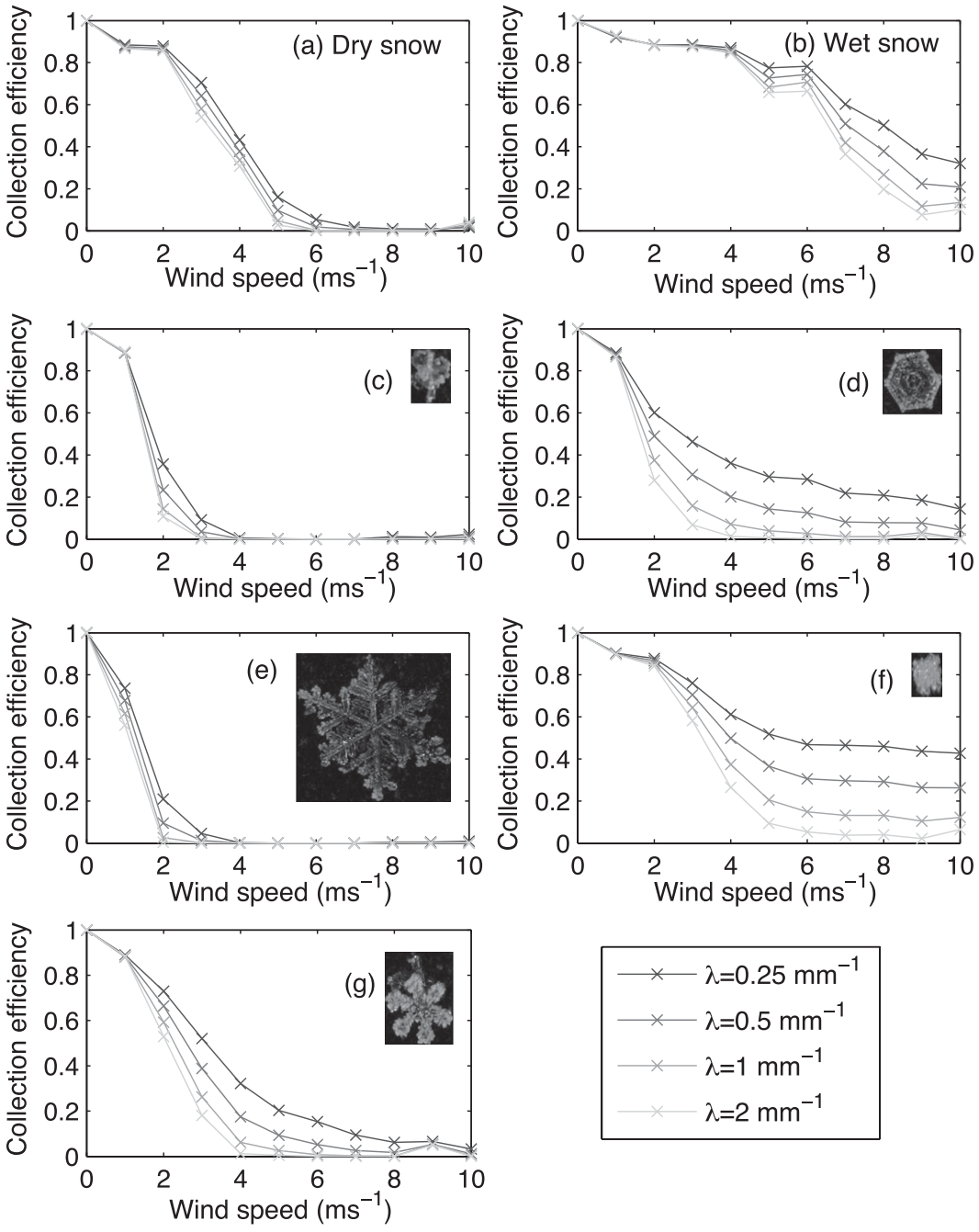


FIG. 10. The collection efficiency variation with wind speed, assuming different slope size distribution values ($\lambda$ = 0.25, 0.5, 1, and 2 mm$^{-1}$) and snowflake types, for (a) dry snow, (b) wet snow, (c) radiating assemblage of plates, (d) hexagonal plates, (e) dendrite, (f) graupel, and (g) heavily rimed dendrite. Pictures of the appropriate snowflake type are included in (c)–(g). The collection efficiency is computed at 1 m s$^{-1}$ increments.

for wet/rimed snow, the minimum size from the size distribution remains constant but the number concentration of small-size snowflakes decreases with increasing wind speed. For example, the number concentration of 0.5-mm snowflakes is 2 times as high at 2 m s$^{-1}$ as at 10 m s$^{-1}$.

### *d. Variation of the slope of the size distribution*

The collection efficiency is proportional to the size distribution of snowflakes falling inside the gauge [Eq. (4)]. Hence, if the parameters of the size distribution are changed, the collection efficiency also varies. Figure 10

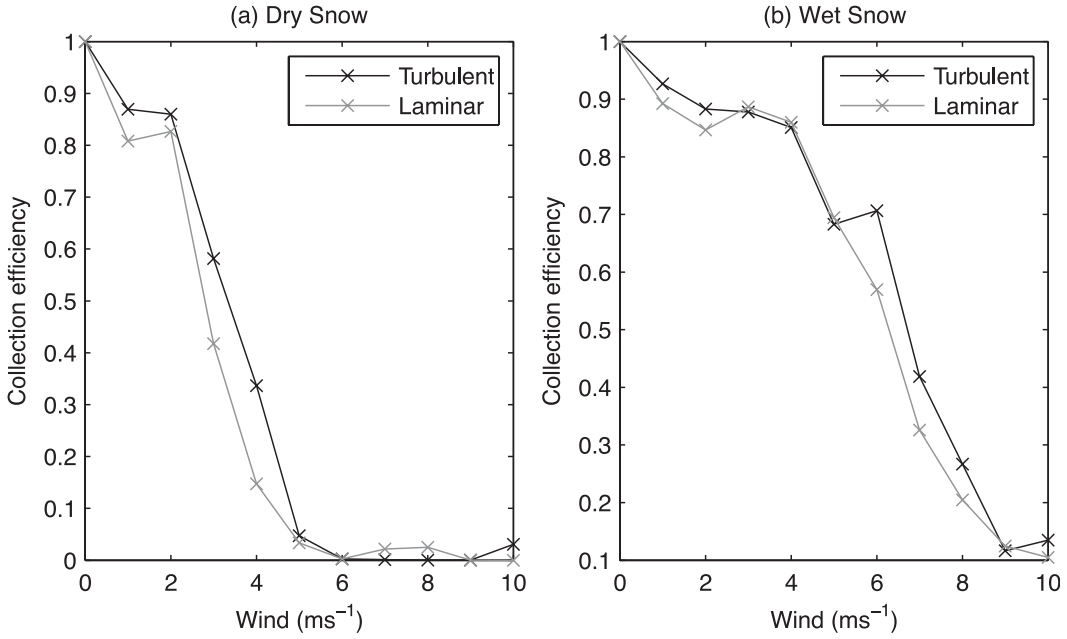


FIG. 11. The collection efficiency of the gauge assuming either turbulent or laminar flow associated with (a) dry snow and (b) wet snow. The slope parameter $\lambda$ is 1 mm$^{-1}$.

shows the changes in the collection efficiency to the variation of the slope of size distribution while the intercept is kept constant.

Figures 10a and 10b show the collection efficiency of dry and wet/rimed snowflakes, respectively. In both cases, the collection efficiency decreases more rapidly with larger values of $\lambda$. The higher the value of the slope of the size distribution is, the lower is the concentration of large snowflakes. Therefore, the values of the collection efficiency are consistent with the results shown in Figs. 8 and 9. Larger snowflakes have higher collection efficiencies than smaller ones for the same wind speed.

The collection efficiency was computed for different crystal types by varying the slope of the size distribution. Note that the collection efficiency of the slow-falling snowflake (Figs. 10a,c,e,g) is small relative to that for fast-falling snowflakes (Figs. 10b,d,f). The collection efficiency of dendrites (Fig. 10e) at 6 m s$^{-1}$ is zero for all values of the slope parameter, whereas the collection efficiency of graupel (Fig. 10f) is about 50% different between a slope parameter of 0.25 and 2 mm h$^{-1}$.

### e. *Turbulent versus laminar flow*

The effect of turbulence on the snow gauge collection efficiency has also been investigated. Figure 11 compares the collection efficiency of dry and wet/rimed snowflakes when falling through either turbulent or laminar flow in the vicinity of the gauge. For both types of snow, the collection efficiencies of the gauge for an assumption of either turbulent or laminar flow are comparable. The collection efficiency is slightly higher when the snowflake falls within a turbulent flow than in a laminar flow, however. This result suggests that the turbulence increases the collection efficiency of the gauge by 10%. Further investigation should be conducted to clarify this issue.

## 5. Observations: 20 February 2010

Snowflakes were collected and photographed during the winter of 2009/10 at the Marshall Test Site near Boulder. The results associated with the 20 February 2010 snowstorm are discussed. In particular, the snowflake types and diameters are compared with the gauge collection efficiency. The number size distributions of snow falling inside and outside the gauge on the basis of the picture analysis are compared with each other. The other snowstorms summarized in Table 1 are presented in section 6.

### a. *Measured collection efficiency*

The gauge collection efficiency was evaluated using the measured precipitation rate from the Geonor in the DFIR. Therefore, the collection efficiency of the Geonor in a single Alter shield is defined as the ratio of the precipitation rate averaged over 10 min measured by the Alter-shielded gauge to that of the Geonor in the DFIR. The wind speed value used to correlate with the

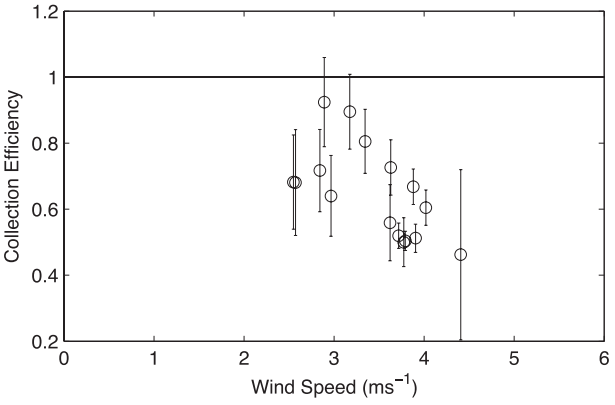


FIG. 12. The collection efficiency of a Geonor placed in a single Alter shield as a function of wind speed for the 20 Feb 2010 snowstorm. The error bar shows the standard deviation of the collection efficiency during the 10-min average.

collection efficiency is also averaged over the 10-min period (at gauge height).

The collection efficiency as a function of the wind speed for that event is shown in Fig. 12. It agrees with previous studies (e.g., Rasmussen et al. 2001) in that the collection efficiency decreases with increasing wind speed, with a large scatter shown within the data. At a given wind speed, the difference in the collection efficiency could be up to 50%. In a similar way, the precipitation rate sometimes varies greatly during the 10-min period. An increase of the collection efficiency is observed between 2.5 and 3 m s$^{-1}$. This increase is mainly due to the type of snowflake. It is discussed later in the section.

### b. Mean diameter

The mean diameter of snowflakes falling in the gauge has been calculated and is shown in Fig. 13 as a function of collection efficiency. In general, the snowflake size increases with decreasing collection efficiency. This is consistent with the theory that larger snowflakes will fall in the gauge as the collection efficiency decreases because larger snowflakes are less affected by the wind than smaller ones. It also depends on the type of snowflake, however. For example, a large dendrite will still fall slower than small graupel.

From observations, each sample has been numbered and classified as ''wet/rimed'' or ''dry'' snow (Fig. 13). There are eight samples of wet/rimed snow and eight samples of dry snow. From Fig. 13, the dry snowflakes are generally larger than the wet/rimed snowflakes. Dry-snow samples 4 and 8 are anomalies, however. Sample 4

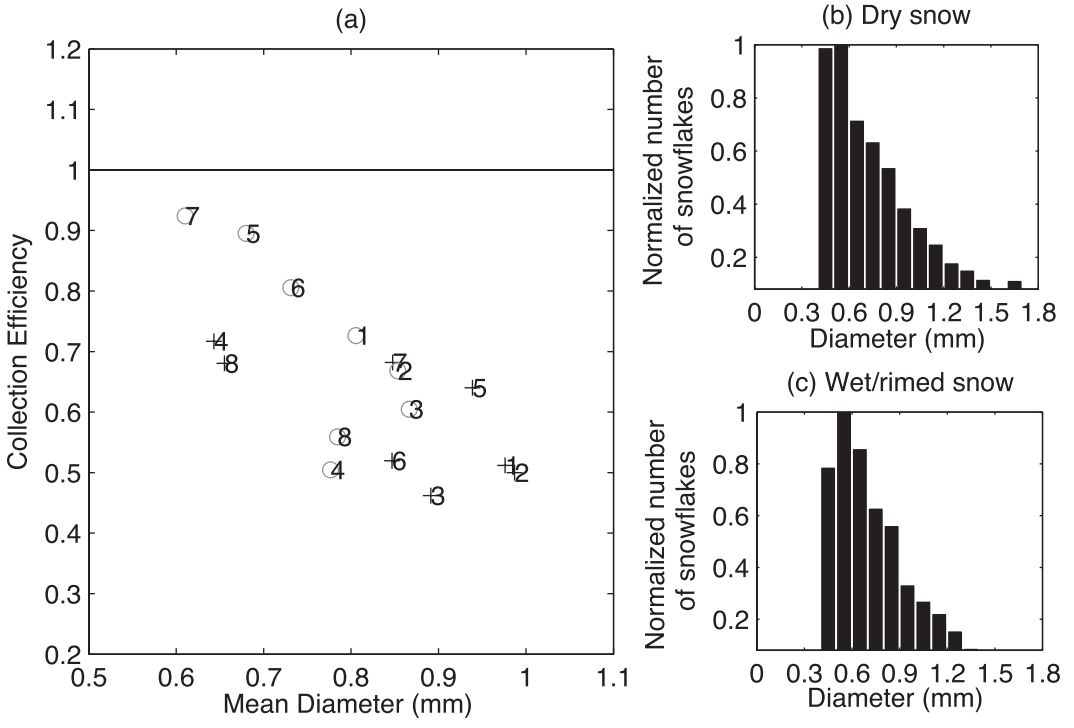


FIG. 13. (a) The collection efficiency of a Geonor in a single Alter shield vs the mean snowflake diameter falling inside the gauge. The gray open circles are for wet/rimed snow, and black plus signs indicate dry snow. There are eight samples of wet/rimed snow and dry snow, numbered from 1 to 8 for each category. Also shown is the normalized number of snowflakes per diameter for (b) dry snow and (c) wet/rimed snow.

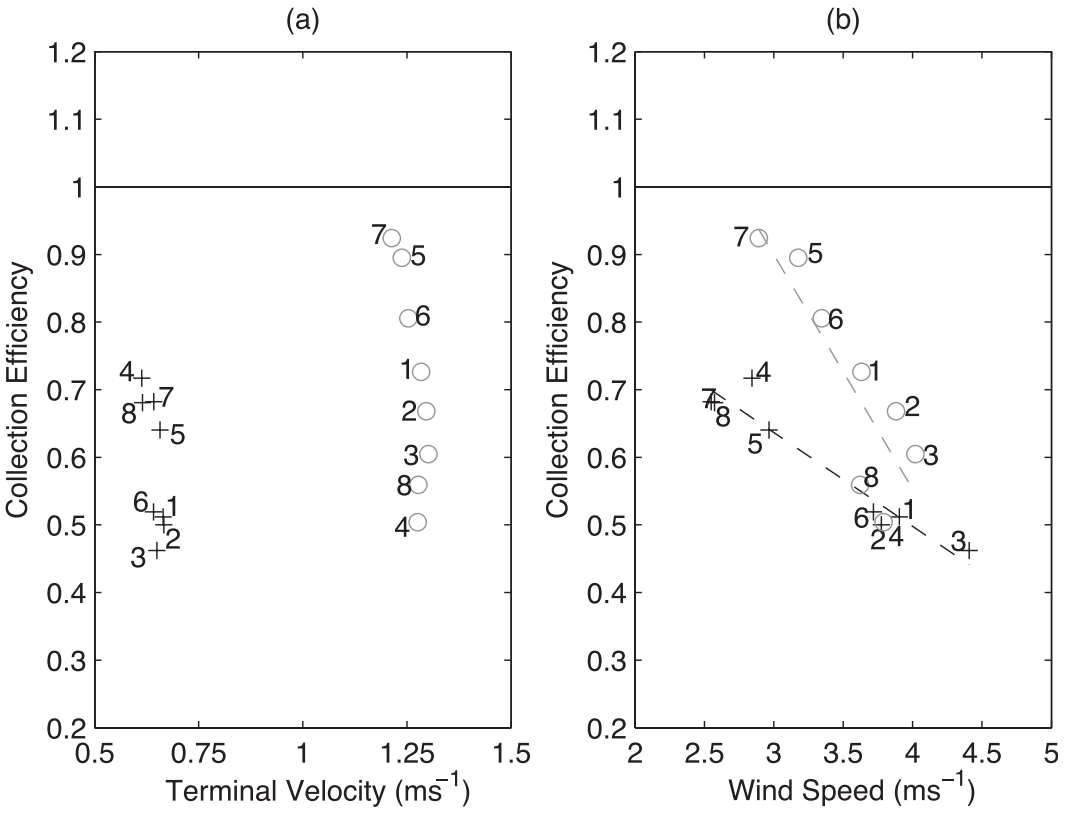


FIG. 14. The collection efficiency of a Geonor in a single Alter shield vs (a) the computed mean terminal velocity of snowflakes falling inside the gauge and (b) the wind speed. The black (gray) dashed lines are the linear-fit curve of dry (wet/rimed) snow samples. The gray open circles are for wet/rimed snow, and black plus signs are for dry snow. There are eight samples of wet/rimed snow and dry snow, numbered from 1 to 8 for each category. These correspond to the samples in Fig. 13.

exhibits lightly rimed dendrites, and sample 8 exhibits radiating assemblage of plates, whereas the other samples depict moderately to heavily rimed dendrites. Overall, the wet/rimed snow category tends to be smaller than the dry snowflakes, as is clearly shown by the size distribution of dry and wet/rimed snow in Figs. 13b and 13c, respectively.

### c. *Computed terminal velocity*

Using the mean diameter of the snowflakes falling inside the gauge, the mean terminal velocity of each sample was computed using Eq. (7). They were divided into dry and wet/rimed snow categories, and the values of the terminal velocity parameters are given in Table 2. Figure 14a shows the computed terminal velocity of the dry and wet/rimed snowflake categories as a function of collection efficiency. The dry snowflakes fall at a terminal velocity that is close to 0.65 m s$^{-1}$, whereas the wet/rimed snowflakes have a terminal velocity that is close to 1.3 m s$^{-1}$, independent of diameter.

The collection efficiency as a function of wind speed and dry and wet/rimed category is shown in Fig. 14b. As expected, the faster-falling snow crystals shown in Fig. 14a are associated with a higher catch efficiency. The slower-falling snowflakes (dry) are associated with lower catch efficiency than are the wet/rimed snow, even if they are larger. For example, dry-snow samples 4 and 5 have lower collection efficiencies than does wet-snow sample 7 for the same wind speed.

### d. *Size distribution inside and outside the gauge*

The number of snowflakes in a given bin size, called the number size distribution, of crystal types falling outside and inside the gauge was also investigated. The mean diameter of each sample of snowflake was studied, and the results are shown in Fig. 13a. It illustrates that small crystals are not effectively collected in high-wind environments, leading to the larger mean crystal sizes when the wind speed is high (i.e., low collection efficiency). Figure 15 shows the snowflake number size distribution inside and outside the gauge. The three

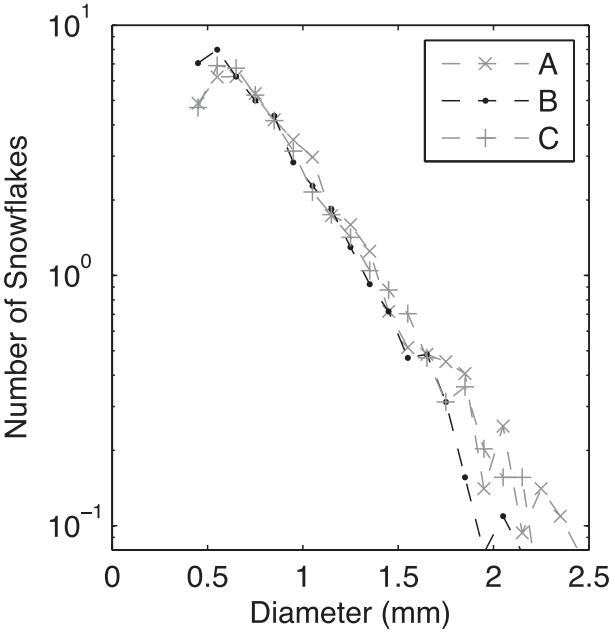


FIG. 15. The size distribution of snowflakes falling into the gauge (label B) in comparison with the ones falling outside the gauge (A and C). The locations represented by these letter labels are shown in Fig. 3.

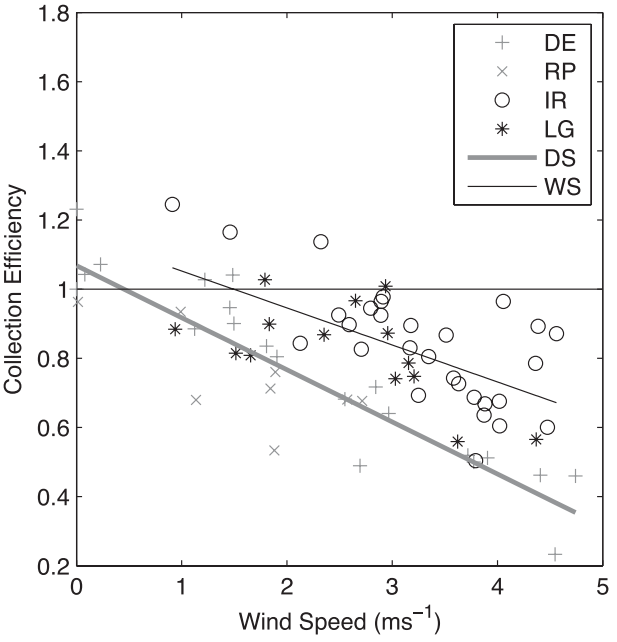


FIG. 16. The collection efficiency of the gauge for the five storms studied (Table 1) as a function of the wind speed. Each sample is associated with the observed crystal types. The gray (black) dashed line is the linear best fit of slow- (fast-) falling snow as indicated by DS (WS). The symbols are given in Table 2, and IR is irregular snowflake type.

number size distributions are comparable. There is a small difference at the tail of the number size distribution in which the number of larger snowflakes is larger outside than inside.

According to a numerical simulation of the flow conducted around a shielded gauge, the deflection of the flow is not symmetric. In general, the shielded gauge slowed the wind downstream of the gauge more than it did upstream. On the upstream side of the gauge, wind speed is higher and the presence of the collection pad may disturb the flow; thus, the snowflake type collected in that region may not have been a good representation of the truth. In a similar way, on the downstream side of the gauge the wind is slowed considerably by the gauge, which is also not an accurate representation of the truth. This observation demonstrates the difficulty in determining the best location and method to collect the true precipitation falling outside the gauge.

## 6. Discussion

### *a. Observations versus theory*

The results presented in the previous sections illustrate the dependence of gauge collection efficiency on snowflake type. The observations of only one storm were analyzed to show the relationship between the snowflake characteristics observed in the field and the gauge collection efficiency. In the following analysis, the data from all five storms are presented (Table 1).

Figure 16 shows the collection efficiency of the Geonor in a single Alter shield as a function of the wind speed for all five storms. Various types of precipitation were observed such as dendrites, three-dimensional snowflakes (i.e., radiating assemblage of plates), irregular ice particles, and graupel. Each sample is associated with a snowflake type. The four snowflake types observed were divided into fast-falling (wet/rimed) and slow-falling (dry) categories according to the terminal velocity as summarized in Rasmussen et al. (1999).

A linear best fit was performed on the observations for both categories (Fig. 16) to compare observations with the theory. It shows that the collection efficiency variation with wind speed for wet/rimed snow is higher than for dry snow for a given wind speed, which is also illustrated by the simulations. The correlation factor of dry snow is 0.90, whereas the wet/rimed snow has a correlation factor of 0.63. This can be explained by the wider variety of crystal types that were included in the particular category. Other snowflake types such as column, capped column, and plates with different degrees of riming were often observed simultaneously with the irregulars. Also, depending on the size of a graupel particle, its terminal velocity may vary greatly. These reasons

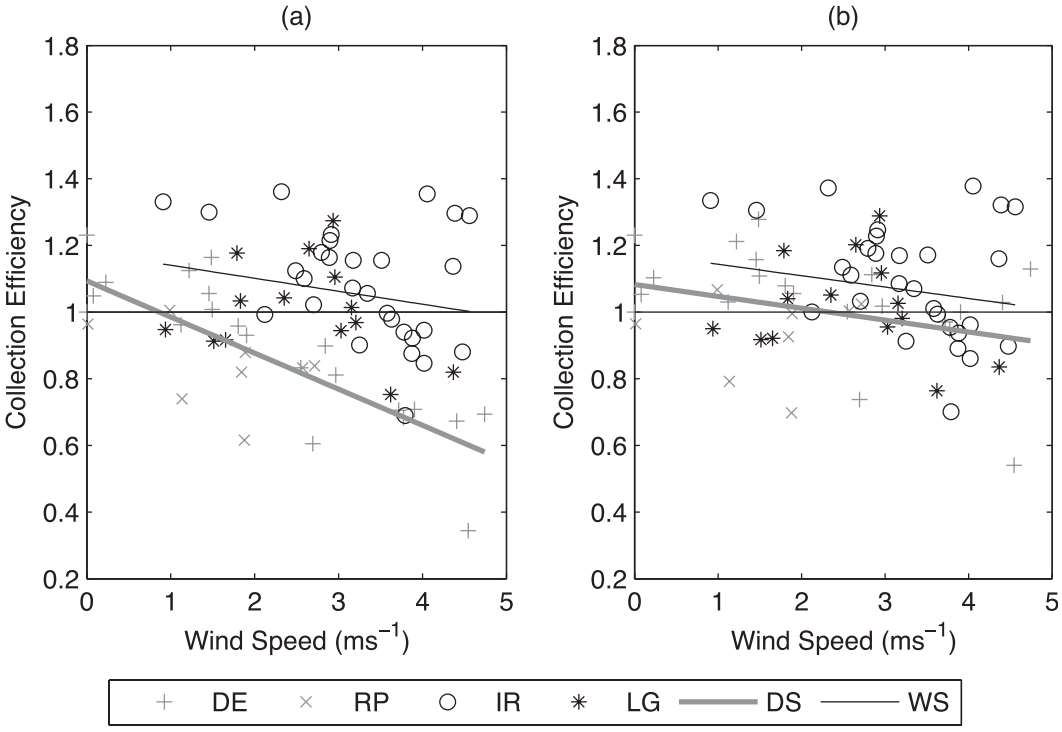


FIG. 17. The corrected collection efficiency (a) computed by assuming the gauge–shield configuration factor [Eq. (11)] and (b) computed by using the correction factor that is based on both gauge–shield and crystal-type factor [Eq. (12)] given in Table 3. Dendrite and radiating assemblage of plates have been corrected with the dry-snow coefficient ($\beta = -5.37$), and graupel and irregulars were corrected with the wet/rimed-snow coefficient ($\beta = -0.3$). In both (a) and (b), the gray (black) dashed line is the linear best fit of slow- (fast-) falling snow as indicated by DS (WS).

could explain the greater scatter in the fast-falling category when compared with the slow-falling one.

### *b. Correction factor*

To account for the decrease in the collection efficiency with increasing wind speed, a correction factor is used to adjust the precipitation rate measured by the gauge. On the basis of the study of Rasmussen et al. (2001), the empirical correction factor relative to the DFIR measurements is

$$\mathrm{Corr}_A = \frac{100}{100 + V\sigma}, \tag{11}$$

where $V$ is the wind speed and $\sigma$ is the gauge configuration parameter. This factor depends on the gauge–shield configuration and the wind speed. For example, the gauge configuration parameter used for the Geonor in the single Alter is $\sigma = -7.1$. As shown in previous studies, the wind speed is an important factor to consider when measuring snowfall. Given the importance of wind speed and shield–gauge geometry, the precipitation rate measured by the Geonor located in a single Alter shield is multiplied by this correction factor to recover the true rate.

Figure 17a shows the collection efficiency using the corrected precipitation rate. Each sample is associated with the main snowflake type observed at that time as in Fig. 16. The correction factor adjusts the collection efficiency of the fast-falling snowflakes better than it does for the slow-falling snowflakes. As can be seen, the corrected data also suggest that the wet/rimed crystal types are overcorrected by the empirical technique and the dry-snow types are undercorrected. Even with the corrected values of the collection efficiency, the precipitation rate associated with slow-falling crystals, such as dendrites and radiating assemblage of plates, is still underestimated. On the other hand, at higher wind speed, the collection efficiency of irregulars is overcorrected by 30%.

The results depicted in Fig. 17a suggest that the correction factor could be improved by modifying Eq. (11) to include the effects of snowflake types. From the theoretical calculations, correction factors have been derived for eight crystal types (Fig. 10). The collection efficiency computed with $\lambda = 1$ mm$^{-1}$ has been approximated by a linear function and combined with Eq. (11). Therefore, the improved the correction factor is

TABLE 3. The computed snowflake-type parameter $\beta$ for the improved correction factor [Eq. (12)].

| Crystal types | Symbol | $\beta$ |
|---|---|---|
| Radiating assemblage of plates | RP | −6.84 |
| Dendrite | DE | −6.98 |
| Heavily rimed dendrites | HD | −6.10 |
| Hexagonal plates | HP | −6.26 |
| Lump graupel | LG | −2.56 |
| Dry snow | DS | −5.37 |
| Wet snow | WS | −0.30 |

$$\mathrm{Corr}_B = \frac{100}{100 + V(\sigma + \beta)}, \tag{12}$$

where $\beta$ is the snowflake-type parameter derived from the theoretical collection efficiency. Table 3 lists the correction factors for the crystal types that were commonly observed.

The corrected data that are based on both the gauge–shield configuration and snowflake types are shown in Fig. 17b. The slow-falling crystal types (dendrite and radiating assemblage of plates) were corrected with the dry-snow correction factor, whereas the fast-falling crystal types (graupel and irregulars) were corrected with the wet/rimed-snow correction factor. The results illustrate that the collection efficiency of the slow-falling snowflakes is improved at higher wind speeds. This result suggests the importance of detailed snowflake-type observations to improve the correction factor of the Geonor in a single Alter shield.

### c. Winter 2009/10

The collection efficiency of the Geonor in a single Alter shield is calculated for the months of December 2009–March 2010, inclusively. The results are shown in Fig. 18 as a box plot. At wind speeds of $<2$ m s$^{-1}$, the median collection efficiency is $>90\%$ but with large scatter. The collection efficiency decreased rapidly from 3 to 7 m s$^{-1}$. At wind speed values of 7 m s$^{-1}$ the collection efficiency is nearly constant at $\sim$0.2.

Figure 18 also shows that the theoretical collection efficiency of dry and wet/rimed snow agrees well with the observations (box plot). At wind speeds between 3 and 7 m s$^{-1}$ the boxes are bound by the wet/rimed and dry-snow curves. The mean theoretical collection efficiency is mainly comparable to the median collection efficiency observed. These two theoretical curves help to explain the scatter in the collection efficiency for a given wind speed. For example, at a wind speed of 5 m s$^{-1}$ the collection efficiency measured by the precipitation gauge varies from 0.2 to 1.0. This variation is mainly explained by the variation in snowflake types. The collection efficiency measured for dry snow at that wind speed value is 0.18, whereas the wet/rimed-snow efficiency is 0.8. The 25th and 75th percentiles lie within the wet/rimed and dry snow, however.

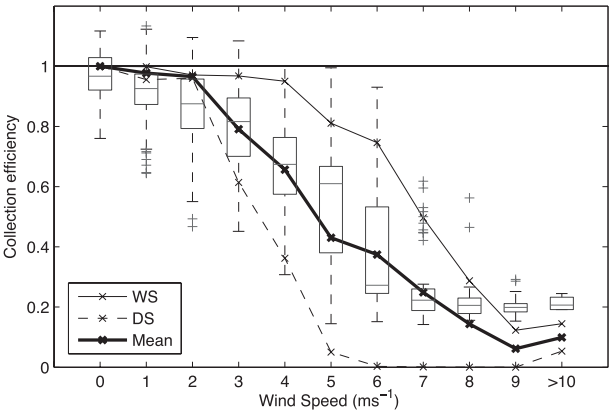


FIG. 18. The collection efficiency of the Geonor in the single Alter shield for winter 2009/10 (Dec–Mar), shown as the box plot. The bottom and top of the box refer to the 25th and 75th percentiles, and the whiskers refer to the 10th and 90th percentiles. The solid (dashed) black line is the theoretical collection of wet/rimed (dry) snow. The mean theoretical efficiency of wet/rimed and dry snow is represented by the thick line.

## 7. Concluding remarks

This study investigated the scatter observed in the collection efficiency of a Geonor placed in a single Alter shield. The results suggest a strong correlation between the crystal types and the gauge collection efficiency. Snowflakes fall at different terminal velocities and therefore interact differently with the deflected flow around the snow gauge. In this study, both observational and theoretical analyses were conducted, and they agree well.

Some experimental errors were also noted. For instance, the observed snow crystal types do not include aggregates. Also, the empirical relationships between snowflake diameter and terminal velocity used to calculate the collection efficiency could be improved by using additional weather instruments to measure terminal velocity such as a Particle Size and Velocity (PARSIVEL) and/or video disdrometer in combination with detailed crystal-type observations.

This study showed that the correction factor currently used operationally to adjust for the bias in the measured precipitation rate needs to be improved. The calculations show that the slow-falling snowflakes are undercorrected and that the fast-falling snowflakes are slightly overcorrected. This finding is particularly important for

wind speeds $>4$ m s$^{-1}$. Correction factors have been suggested for seven different types of snowflakes that could be divided into two categories: wet/rimed snow (fast falling) and dry snow (slow falling).

Further experiments should be conducted to compare the terminal velocity measured by a disdrometer with the collection efficiency of the snow gauge. It may be possible to derive a threshold value between slow- and fast-falling snowflakes. On the other hand, the temperature could also help in determining the speed of the snowflakes. Wet snow mainly occurs at temperatures near 0°C, whereas dry snow occurs at colder temperatures (Brandes et al. 2008). At colder temperatures, however, it is difficult to determine whether the snowflakes are rimed, and there is a significant difference between the terminal velocity of a dry snowflake and a rimed snowflake. Also, this experiment could be repeated with a Geonor in a DFIR at two different locations on the site. This could help in estimating the efficiency of the DFIR shield.

The impact of turbulence on the collection efficiency of the gauge is not clear. A previous study by Nespor and Sevruk (1999) suggested that turbulence has an effect on the snowflake trajectory by adding an extra term in the particle Reynolds number. It was assumed that the effect of turbulence is only taken into account by the simulated flow and not in the drag coefficient, however. The drag coefficient depends only on the crystal types and not on the surrounding environment. Note that a significant difference was not observed in the collection efficiency between turbulent or laminar flow. Further studies should be conducted on the turbulent effect on the snowflake trajectory in the vicinity of a precipitation gauge, however. Such studies could help to explain some of the results obtained in this initial study.

Overall, this study shows the strong impact of crystal types on the gauge collection efficiency and helps to explain the large scatter in the data. These key findings could have an impact on, for instance, long-term snowfall measurements. In particular, warm regions experiencing wet snow could receive more snow than cold regions as a result of the higher collection efficiency of wet snow in comparison with dry snow. This study has also increased our understanding of the factors responsible for the difficulty in measuring snow.

*Acknowledgments.* We thank the Advanced Study Program and the Research Applications Laboratory at the National Center for Atmospheric Research (NCAR) for the financial support needed to accomplish this work. NCAR is sponsored by the National Science Foundation. We thank Al Jachcik for building the experimental setup, Sara Ziegler for analyzing snowflake pictures, and Andy Gaydos for processing data. We also thank Jennifer Black for helping with data analysis and Prof. Stéphane Etienne for insightful advice with computational fluid dynamic approaches. Last, we thank the anonymous reviewers for their constructive comments.

## REFERENCES

Alter, J. C., 1937: Shielded storage precipitation gauges. *Mon. Wea. Rev.,* **65,** 262–265.

Bakkehøi, S., K. Øien, and E. J. Førland, 1985: An automatic precipitation gauge based on vibrating-wire strain gauges. *Nord. Hydrol.,* **16,** 193–202.

Brandes, E. A., K. Ikeda, G. Zhang, M. Schonhuber, and R. Rasmussen, 2007: A statistical and physical description of hydrometeor distributions in Colorado snowstorms using a video disdrometer. *J. Appl. Meteor. Climatol.,* **46,** 634–650.

——, ——, G. Thompson, and M. Schonhuber, 2008: Aggregate terminal velocity/temperature relations. *J. Appl. Meteor. Climatol.,* **47,** 2729–2736.

Goodison, B. E., P. Louie, and D. Yang, 1998: WMO solid precipitation measurement intercomparison: Final report. WMO Tech. Doc. 872, WMO, Geneva, Switzerland, 212 pp.

Groisman, P. Ya., and D. R. Legates, 1994: The accuracy of United States precipitation data. *Bull. Amer. Meteor. Soc.,* **75,** 215–227.

——, V. V. Koknaeva, T. A. Belokrylova, and T. R. Karl, 1991: Overcoming biases of precipitation measurement: A history of the USSR experience. *Bull. Amer. Meteor. Soc.,* **72,** 1725–1733.

Hanson, C. L., F. B. Pierson, and G. L. Johnson, 2004: Dual-gauge system for measuring precipitation: Historical development and use. *J. Hydrol. Eng.,* **9,** 350–359.

Houze, R. A., P. V. Hobbs, and P. H. Herzegh, 1979: Size distributions of precipitation particles in frontal clouds. *J. Atmos. Sci.,* **36,** 156–162.

Locatelli, J. D., and P. V. Hobbs, 1974: Fall speeds and masses of solid precipitation particles. *J. Geophys. Res.,* **79,** 2185–2197.

Marshall, J. S., and W. M. Palmer, 1948: The distribution of raindrops with size. *J. Meteor.,* **5,** 165–166.

Nespor, V., and B. Sevruk, 1999: Estimation of wind-induced error of rainfall gauge measurements using a numerical simulation. *J. Atmos. Oceanic Technol.,* **16,** 450–464.

Newman, A. J., and P. A. Kucera, 2005: Gauging rainfall. *Fluent News Fall Newsletter,* No. 14, The Fluent Group, 12–13.

Nipher, F. E., 1878: On the determination of the true rainfall in elevated gauges. *Proc. 27th Meeting of the American Association for the Advancement of Science,* St. Louis, MO, The American Association for the Advancement of Science, 103–108.

Passarelli, R. E., 1978: Theoretical and observational study of snow-size spectra and snowflake aggregation efficiencies. *J. Atmos. Sci.,* **35,** 882–889.

Pruppacher, H. R., and J. D. Klett, 1997: *Microphysics of Clouds and Precipitation.* 2nd ed. Kluwer Academic, 976 pp.

Rasmussen, R. M., J. Vivekanandan, J. Cole, B. Meyers, and C. Masters, 1999: The estimation of snowfall rate using visibility. *J. Appl. Meteor.,* **38,** 1542–1563.

——, and Coauthors, 2001: Weather Support to Deicing Decision Making (WSDDM): A winter weather nowcasting system. *Bull. Amer. Meteor. Soc.,* **82,** 579–595.

——, and Coauthors, 2012: How well are we measuring snow? The NOAA/FAA/NCAR winter precipitation test bed. *Bull. Amer. Meteor. Soc.,* in press.

Sekhon, R. S., and R. C. Srivastava, 1970: Snow size spectra radar reflectivity. *J. Atmos. Sci.,* **27,** 299–307.

Sevruk, B., M. Ondás, and M. Chvíla, 2009: The WMO precipitation measurement intercomparisons. *Atmos. Res.,* **92,** 376–380.

Smith, G., 2009: The relationship between snowfall catch efficiency and wind speed for the Geonor T-200B precipitation gauge utilizing various wind shield configurations. *Proc. 77th Western Snow Conf.,* Canmore, Alberta, Canada, Western Snow Conference, 115–121.

Yang, D., and Coauthors, 1995: Accuracy of Tretyakov precipitation gauge: Result of WMO intercomparison. *Hydrol. Processes,* **9,** 877–895.

——, B. Goodison, and J. R. Metcalf, 1998: Accuracy of NWS 8″ standard nonrecording precipitation gauge: Results and application of WMO intercomparison. *J. Atmos. Oceanic Technol.,* **15,** 54–68.

——, and Coauthors, 1999: Quantification of precipitation measurement discontinuity induced by wind shields on national gauges. *Water Resour. Res.,* **35,** 491–508.

——, D. Kane, Z. Zhang, D. Legates, and B. Goodison, 2005: Bias corrections of long-term (1973–2004) daily precipitation data over the northern regions. *Geophys. Res. Lett.,* **32,** L19501, doi:10.1029/2005GL024057.

Yuter, S. E., D. E. Kingsmill, L. B. Nance, and M. Löffler-Mang, 2006: Observations of precipitation size and fall speed characteristics within coexisting rain and wet snow. *J. Appl. Meteor. Climatol.,* **45,** 1450–1464.